Grain boundary-induced plasticity during thin film buckling

Benjamin Bertin, J. Durinck, Jean Grilhé, Jérôme Colin

▶ **To cite this version:**

Benjamin Bertin, J. Durinck, Jean Grilhé, Jérôme Colin. Grain boundary-induced plasticity during thin film buckling. Mechanics of Materials, 2021, 155, pp.103761. 10.1016/j.mechmat.2021.103761 . hal-03155497

HAL Id: hal-03155497
https://hal.science/hal-03155497

Submitted on 3 Feb 2023

HAL is a multi-disciplinary open access archive for the deposit and dissemination of scientific research documents, whether they are published or not. The documents may come from teaching and research institutions in France or abroad, or from public or private research centers.

L'archive ouverte pluridisciplinaire **HAL**, est destinée au dépôt et à la diffusion de documents scientifiques de niveau recherche, publiés ou non, émanant des établissements d'enseignement et de recherche français ou étrangers, des laboratoires publics ou privés.

Distributed under a Creative Commons Attribution - NonCommercial 4.0 International License

Version of Record: https://www.sciencedirect.com/science/article/pii/S0167663621000193
Manuscript_7fa34834ed8aa0fab3a1ea8a2e1a06af

Grain boundary-induced plasticity during thin film buckling

Benjamin Bertin, Julien Durinck, Jean Grilhé, Jérôme Colin

Institut Pprime, Université de Poitiers, CNRS, TSA 41123 86073 Poitiers Cedex 9, France.

Abstract

The effect of grain boundaries (GB) on the buckling of an Al thin film delaminated from its substrate is investigated by means of molecular dynamics simulations at finite temperature. It is evidenced that the GB localizes the plasticity and deeply modifies the profile of the buckled thin film through the formation of a vertical fold at the location of the initial GB. Several plasticity mechanisms have been also described such as the development of extrinsic faults or the formation of uncommon C'D and CD' dislocations. In this context, the folding angle and plastic strain in the film have been analyzed through a careful counting of the emerging dislocations at the film surfaces. The buckling profile of the film has been then analytically determined in the framework of the Föppl-von Karman's (FvK) theory of thin plates and successfully compared with the simulated ones. The modifications of the film pattern in light of the different plastic (dislocations) and elastic (buckling) phenomena are finally discussed.

Keywords: Thin film, Buckling, Grain boundaries, Dislocation, Atomistic simulations, Folding

1. Introduction

The control of the mechanical properties of thin films deposited on substrates, coatings and multilayers is of paramount importance because of the numerous applications of such composite structures in materials science, metallurgy and more broadly in engineering. Within these different research communities, it is now well admitted that a large amount of strain [1, 2, 3] may develop

© 2021 published by Elsevier. This manuscript is made available under the CC BY NC user license
https://creativecommons.org/licenses/by-nc/4.0/

in the above cited structures, resulting from the material fabrication process, the lattice or dilatation coefficient mismatches, for example, which can lead to the delamination of the film/substrate interfaces and to the final buckling of the layers from their substrates. In the framework of the well-established Föppl-von Karman's (FvK) theory of thin plates, a number of buckling patterns have been characterized for thin films already partially delaminated from their substrates, at the mesoscopic scale, among which the circular blisters, straight-sided or telephone-core buckles are most often cited (see [4, 5, 6, 7, 8, 9] and references therein). More precisely, the different profiles of the delaminated films have been determined and successfully compared with the experimental ones analyzed by optical or atomic force microscopies. Likewise, the thresholds of critical strain required for buckling have been determined for the various geometries. The further step of these studies has been to simultaneously consider the interface delamination and the film buckling. Recently, combining non-linear plate deformation with a cohesive zone model, finite element (FE) simulations have been performed and a worm-like propagation mode has been identified for the blisters [10]. Considering interface steps, the possibility of buckle deviation from their initial trajectory has been also discussed from FE simulations [11].

In this context of mesoscale studies of multilayer deformation, the question of the influence of plasticity seems to naturally emerge for both mono and polycrystalline layers. Indeed, it has already been observed that cracks may appear at the top or at the edges of straight-sided buckles for Cr, Ti and Cu/Zr thin films deposited on compliant substrates [12, 13, 14]. The same phenomenon has also been observed after buckling for Cu/Nb and Cu/Cr multilayered structures [15, 16]. Likewise, for Y_2O_3 or Au thin films deposited on Si substrates, a plastic folding effect has been observed [17, 18] to take place at the top side or at the circumference of the buckles, this folding being analyzed in terms of low angle tilt-boundaries that can be represented by a vertical row of edge dislocations [19]. It is finally to emphasize that the nucleation and gliding of dislocations from the top of the buckles to the edges have also been characterized, through molecular dynamics simulations, to substantially decrease the deflection of the

buckles [20].

Thus, it clearly appears from the above cited literature that both plasticity and buckling phenomena are deeply connected and should be simultaneously treated to describe the morphological evolution of the crystalline thin films deposited on substrates under compressive strain. It is the topic of the present work to investigate the evolution of the already delaminated part of an initially planar thin film of a fcc metal on a model substrate and submitted to increasing strain. Molecular dynamics (MD) simulations at finite temperature are reported in the case where a grain boundary (GB) is lying into the delaminated film. The evolution of the dislocations composing the GB is carefully described and the key parameters resulting from the plastic deformation, i.e. a folding angle and a plastic strain, are then included into an analytical model of elastic buckling which is found to capture the observed shape change of the film.

2. Numerical details

An initially planar Al thin film of length $L_x = 1620.00\,\mathring{A}$ and height $h = 111.24\,\mathring{A}$ in the $(0xz)$ plane, delaminated from a model substrate on a length $b_1 + b_2$, is considered in Fig. (1). Along $(0y)$ axis, periodic boundary conditions are applied such that length of the system can be considered as infinite in this direction. This system which is composed of approximately 220,000 atoms has been generated with the help of the LAMMPS code [21], where the atomic interactions are mimicked by an EAM potential for Al [22], with $a = 4.05\,\mathring{A}$, the lattice parameter of Al. A low angle tilt-boundary has been introduced into the Al crystal in such a way that it is in agreement with experimental observations [23]. More precisely, the grain 1 (regions 0 and 1) is oriented along $(Ox_1)\,//\,[55\bar{1}]$ and $(Oz_1)\,//\,[1\,1\,10]$ while the grain 2 (regions 2 and 3) is oriented along (Ox_2) // $[551]$ and (Oz_2) // $[\bar{1}\bar{1}10]$ [24, 25, 26] such that a $\Sigma 51$ (551) GB, composed of 10 perfect edge dislocations, is generated accommodating the orientation mismatch between both grains [27, 19]. In order to optimize the density at the GB, void spaces of less than half of the lattice parameter a, left

by the rough GB construction, are replaced by only one atom. No substrate has been directly introduced in the simulation but its influence has been implicitly considered using clamping conditions at both extremities of the thin film such that the regions 0 and 3 in Fig. (1) correspond to the sticking parts of film to the substrate, assumed to remain planar during the compression test.

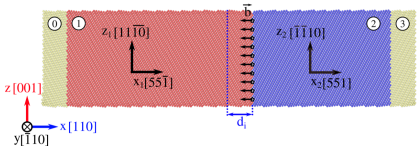

Figure 1: Sketch (not to scale) of the simulation box composed of four regions of the film deposited on a rigid substrate (not shown). The regions $(0, 1)$ and $(2, 3)$, correspond to the disoriented grains 1 and 2, respectively, between which a $\Sigma 51$ (551) GB is positioned at a distance d_i from the center. The regions 0 and 3 are planar and stick to the substrate, the regions 1 and 2 are assumed to be delaminated from the substrate. This GB is composed of a row of 10 perfect edge dislocations where the Burgers vector $\frac{a}{2}[\bar{1}\bar{1}0]$ for each dislocation of the row is displayed (black arrows).

The resulting two-grain crystal, in the low angle tilt-boundary limit, can finally be assimilated to a $x = [110]$, $y = [\bar{1}10]$ and $z = [001]$ oriented thin film, where the GB is constituted by a row of perfect $\frac{a}{2}[\bar{1}\bar{1}0]$ dislocations lying in the (Oyz) plane, at the GB position d from the plane of symmetry of the film (see Fig. 1). In the following, three positions d_i of the GB have been tested, i.e. $d_0 = 0$ for the configuration where the GB is located at the middle of the delaminated film (labeled symmetric configuration) and $d_1 = 86.13\,\mathring{A}$ and $d_2 = 169.32\mathring{A}$ for the configurations where the GB is shifted with respect to the middle of the film (labeled asymmetric configurations). In a first time, only the symmetric case where the GB is located at the middle of the film (d_0) is studied, the asymmetric cases (d_1 and d_2) will be discussed later. Once the film is built, a first energy minimization, with the help of a conjugate gradient algorithm [21], is applied to the system which is then heated at 300 K during 100 ps in a NPT thermodynamics ensemble with zero pressure P. The strain

is applied along (Ox) with increments of -0.01% from $\varepsilon_a = -1.3\%$, assumed to be lower than the critical strain for buckling [4, 5, 7], to $\varepsilon_a = -3\%$. The edges of the film are clamped after application of the strain by imposing no further displacement for all the atoms in regions 0 and 3. At each strain step, a molecular dynamics is performed during 10 ps using a NVT thermostat at $T = 300$ K. In order to obtain a more reliable statistics for our results, three simulations with different initial sets of the atom velocities are performed for each configuration corresponding to a given grain boundary position. In each case, it has been confirmed that the plasticity mechanisms do not depend on these initial atom velocities. However, the strain levels at which the dislocations are nucleated are slightly different from one simulation to another.

3. Plasticity mechanism analysis

The plasticity of the film under increasing strain can be now analyzed for the $\Sigma 51(551)$ GB in the symmetric configuration [24, 25, 26]. In agreement with previous works [4, 5, 7, 8], it has been observed but not shown during the first steps of compression beyond (in absolute value) $\varepsilon_a = -1.65\%$ that the film first buckles before any plasticity mechanism is activated, the upper part of the film beyond the midplane being in tension while the lower part being in compression [28, 20]. It is also underlined that when the applied strain is large enough, the dislocations are nucleated from the GB through the formation of extrinsic stacking faults (ESF) for the compressed area due to the anti-twinning orientation and of intrinsic stacking faults (ISF) for the tensile area due to the twinning orientation, these stacking fault being recovered when they are swept out by further dislocations nucleated under increasing strain [29, 30]. In the following, the Thompson's notations [31] have been used to describe the plasticity developing into the film, the tetrahedron orientation being given in Fig (2). Fig. (3)a shows the final configuration of the system after buckling and folding and Fig. (3)b displays the strain distribution inside the film, where compression and tensile regions are evidenced. It is observed that in the upper and lower central

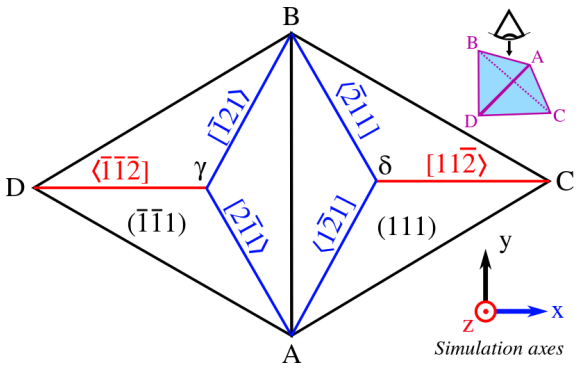

Figure 2: Top view of the Thompson's tetrahedron whose orientation corresponds to the orientation of the film. The inset (upper right region) represents the three-dimensional tetrahedron.

parts of the film, the tension and compression are high and both decrease (in absolute value) in the regions shifted with respect to the central one until the part of the film where the free-surface curvature changes its sign is reached. This can qualitatively explains why the plasticity mechanisms will be found in the following more active when the GB is in the central position compared to the shifted ones. Fig. (3)c shows the film once the clamped conditions are released and after the folding and plastic deformation appear. This configuration will be used in the next section to determine the plastic deformation.

Figs. (4) show the plastic mechanisms at different strain levels near the grain boundary, leading to the folding of the film. From Fig. (4)a, it can be observed that in the lower part of the film under compression, two Shockley's dislocations ($A\gamma$ and $B\gamma$) are nucleated in the grain 1 from the second perfect dislocation of the GB (the dislocations are counted from the lower surface of the film in the following). These two Shockley's dislocations are the result of the dissociation of a γD dislocation to which a maximum resolved shear stress is applied but for which slip in the $(\bar{1}\bar{1}1)$ is inhibited due to the anti-twinning orientation. Both $A\gamma$ and $B\gamma$ dislocations then glide concomitantly in two successive $(\bar{1}\bar{1}1)$ planes, leaving a Frank's dislocation ($C\gamma$) at the GB and leading to the formation of an

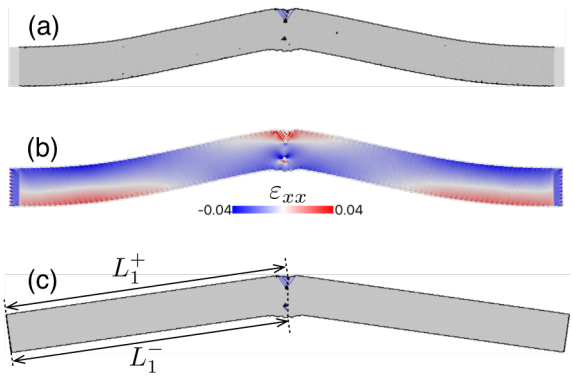

Figure 3: Thin film deformed at $\varepsilon_a = -2.49\%$. (a) Buckled configuration with the colors of the atoms corresponding to the local atomic stacking (fcc = grey, hcp = blue, other = black), (b) strain distribution ε_{xx} in the buckled thin film and (c) unclamped released configuration after folding and plastic deformation took place.

ESF. It can be emphasized at this point that this mechanism is observed for the first to the sixth dislocations of the GB, the Burgers vectors of the emitted and of the remaining dislocations depending on the grain in which the mechanism occurs. Indeed, in the grain 2, the δA and δB dislocations are nucleated from the CD dislocation and then glide concomitantly in two successive (111) planes leaving a δD dislocation at the GB, as it can be shown in Fig. (4)c. These two reactions can be summarized as:

$$CD \rightarrow A\gamma + B\gamma + C\gamma, \text{ for grain 1,} \quad (1)$$

$$CD \rightarrow \delta A + \delta B + \delta D, \text{ for grain 2.} \quad (2)$$

When ε_a reaches -2.42%, a first partial dislocation $C\delta$ is then nucleated from the δD in grain 2 and glides in the (111) plane, changing in Fig. (4)b, the ESF into an ISF. A particular dislocation with a Burgers vector $\frac{1}{6}[\bar{1}\bar{1}\bar{4}]$ remains in the GB. This atypical dislocation, labeled $C'D$ in the following, has already been observed and described [32] and can be seen as a partial dislocation with the same Burgers vector length ($a\frac{\sqrt{2}}{2}$) as that of a perfect dislocation [33]. The same decomposition occurs in grain 1 for the $C\gamma$ dislocation, where a γD partial dislocation is nucleated, leaving a CD' dislocation at the GB of Burgers vector

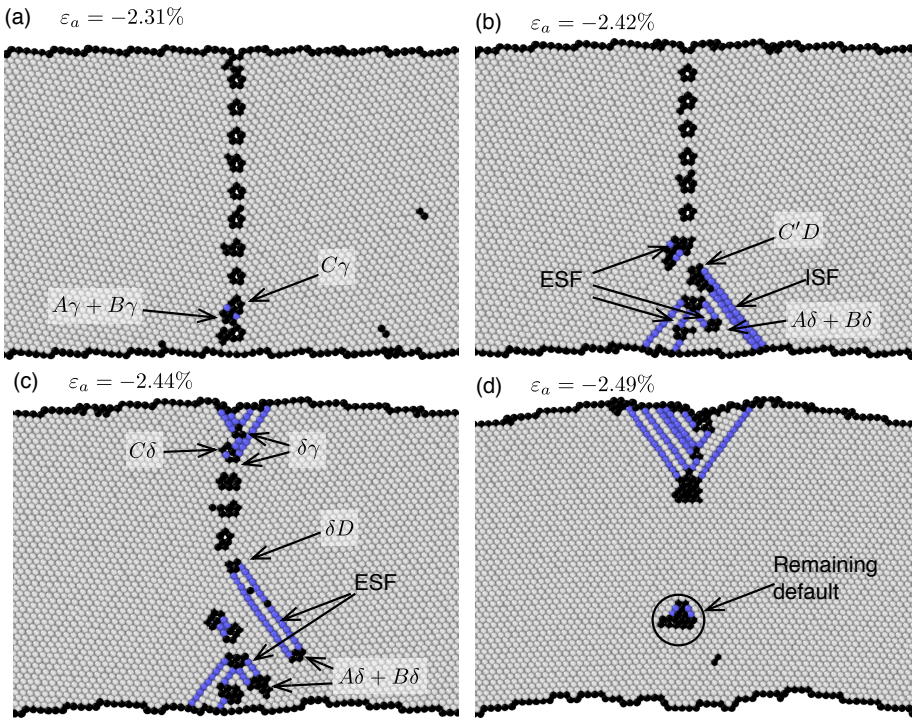

Figure 4: Snapshots of the thin film evolution near the Σ 51 (551) GB at $d = 0$. (a) In the lower compressive region of the film, $A\gamma$ and $B\gamma$ dislocations are nucleated in grain 1 from one CD dislocation of the GB, producing a γD total slip displacement and leaving a $C\gamma$ dislocation at the GB. (b) The glide of $A\gamma$ and $B\gamma$ dislocations leads to the formation of an ESF in grain 1. The same mechanism operates in grain 2 (see c) with the glide of δA and δB dislocations leaving a δD dislocation in the GB. A $C\delta$ dislocation has been nucleated from one remaining δD dislocation in the GB and has glided in grain 2, changing an ESF into an ISF. (c) In the upper tensile region, a $C\delta$ dislocation and a $D\gamma$ dislocation (not shown in this snapshot) have glided in grain 1 and grain 2 respectively, leaving a $\delta\gamma$ Frank's dislocation in the GB. (d) The perfect crystal is partially recovered in the compressive region, only one default resulting from the recombination of dislocations that remains in the GB is still present. Some stacking faults are present in the tensile region. The colors of the atoms correspond to the local atomic stacking (fcc = grey, hcp = blue, other = black).

$\frac{1}{6}[\bar{1}\bar{1}4]$, the two mechanisms in the grains being written as:

$$C\gamma \quad \rightarrow \quad \gamma D + CD', \text{ for grain 1,} \tag{3}$$

$$\delta D \quad \rightarrow \quad C\delta + C'D, \text{ for grain 2.} \tag{4}$$

Finally, from our simulations (not shown), it appears that the plastic mechanisms taking place later in the compressed area are too complex to be described step-by-step. But in a general way, it can be stated that the remaining dislocations recombine and/or dissociate into partial dislocations which glide toward the lower surface, contributing to fully or partially removing the GB and recovering the perfect crystal. However, in Fig. (4)d, a few defaults still remain into the film despite these dislocation nucleations, glides and recombinations. In the upper tensile region now, when the applied strain reaches -2.44%, two partial dislocations $D\gamma$ are nucleated (Fig. (4)c) from the vicinal steps of the upper free-surface of the film, in the grain 2, and glide in a $(\bar{1}\bar{1}1)$ plane until they reach the first two CD perfect dislocations of the GB. The CD and $D\gamma$ dislocations recombine then into a $C\gamma$ Frank's dislocation, this $C\gamma$ dissociating instantaneously into a $\delta\gamma$ stair-rod dislocation and a $C\delta$ partial dislocation as,

$$D\gamma + CD \rightarrow C\gamma \rightarrow \delta\gamma + C\delta. \tag{5}$$

The $C\delta$ finally glides into a (111) plane in the grain 1 until it reaches the top surface. The remaining ISF resulting from the gliding of these leading partial dislocations are observed in Fig. (4)d to adopt a "V" shape. It can finally be emphasized that in both symmetric and asymmetric GB configurations and when the applied strain is large enough (not shown), these ISFs can be annihilated by the nucleation of trailing partial dislocations from the upper surface.

When the GB is shifted from the center of the delaminated film, simulations exhibit the same plastic mechanisms initiated from and/or localized near the GB. The main differences with the symmetrical configuration lie in the size decrease of the upper tensile region with respect to the size of the lower region in compression and in the decrease of the stress gradient through the thickness of the film. A small decrease in the plastic deformation is also observed for the same level of applied strain as the GB is shifted. Once the plasticity mechanisms

activated at the microscopic scale have been identified, the resulting shape modification at the upper scale of the film can be now analyzed. It is the topic of the next part of this work.

4. Dislocation-induced folding and plastic strain

In order to estimate the plastic deformation resulting from the dislocation emission, two equivalent procedures have been used. They both consist in the determination of the length variations with respect to the initial half-length L_0 of the film, of the upper and lower surfaces, ΔL_i^+ and ΔL_i^-, respectively, for the grain i, with $i = 1, 2$ (Fig. (5)a).

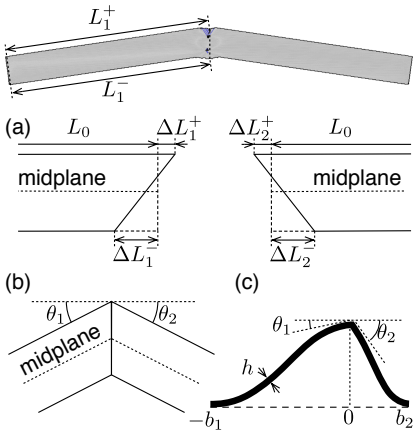

Figure 5: Sketch of the shape modification of the film due to plasticity. (a) Resulting shape of each grain after dislocation gliding compared to the initial shape of half-length L_0. (b) Final shape of the folded film. (c) Schematic of a buckled and folded thin film of length $b_1 + b_2$ and thickness h. The folding angle is $\theta_f = \pi - \theta_1 - \theta_2$.

The first one is related to the plastic mechanisms that take place during buckling and consists in counting the number of the emitted dislocations. When a dislocation nucleated from the GB reaches the upper or lower free-surface of the film, its length is reduced or increased by the quantity corresponding to the projection of the Burgers vector along the surface direction of the film. ΔL_i^+ and ΔL_i^- are then determined by summing up all the Burgers vector projections of

the dislocations emerging on the upper (+) and lower (-) surfaces for each grain i. The second one consists in a direct measurement of the length variation due to plastic deformation. To do so, once the film has buckled, the applied strain has been removed and the clamping conditions at both extremities of the film have been released in such a way that the elastic strain and the bending moment cancels, leading to the configuration shown in Fig. (3)c. The final lengths L_i^+ and L_i^- of the upper and lower free-surfaces have been measured for both grains ($i = 1, 2$) and compared with the initial half-length of the planar film L_0. The variations (taken to be positive quantities) of the upper and lower surfaces of the grain i are calculated as $\Delta L_i^+ = \left|L_i^+ - L_0\right|$ and $\Delta L_i^- = \left|L_i^- - L_0\right|$, respectively, with $i = 1, 2$. Assuming a linear variation of the lengths between the upper and lower surfaces, the grain modification from a rectangle to a trapezoidal shape leads to the folding of the film in Fig. (5)b at the initial position of the GB. This folding is characterized by an angle $\theta_i > 0$ in grain i determined as follows:

$$\theta_i = \arctan\left(\frac{\Delta L_i^+ + \Delta L_i^-}{h}\right), \tag{6}$$

and the total plastic deformation is responsible for the modification ΔL_i^m of the length of the film calculated in the midplane by:

$$\Delta L_i^m = \frac{\Delta L_i^- - \Delta L_i^+}{2}, \tag{7}$$

with $i = 1, 2$. In order to verify the accuracy of this simple model, the key quantities ΔL_i^j, with $i = 1, 2$ and $j = \pm$, determined from the dislocation counting (d) have been compared in Table 1 with the same quantities directly estimated from the measurement of the length variations of the film taken from the simulations (s). It appears from this Table 1 that the model gives relatively accurate values of the length variations considering that only one dislocation may modify the final results of a few percent and, the determination of the length variations from the simulations also generates an error of a few percent. Thus, it justifies that the dislocations from the GB are responsible for the folding of the film of an angle θ_f and may also explain the presence of a plastic strain

GB	ΔL_1^+ (Å)		ΔL_2^+ (Å)		ΔL_2^- (Å)		ΔL_2^- (Å)	
position	d	s	d	s	d	s	d	s
d_0	9.07	10.64	9.07	10.32	4.54	4.95	4.54	4.91
d_1	5.39	4.62	5.29	4.63	3.40	3.37	3.40	2.99
d_2	6.81	7.04	5.67	5.71	3.40	3.97	3.40	3.50

Table 1: Comparison between the different length variations ΔL_i^j obtained from the dislocation model ("d" column) and from the simulations ("s" column) for different GB positions d_k, with $i = 1, 2$, $j = \pm$ and $k = 0, 1, 2$.

ε_p in the midplane, whose expressions are given by:

$$\theta_f = \pi - \theta_1 - \theta_2, \tag{8}$$

$$\varepsilon_p = \frac{\Delta L_1^m + \Delta L_2^m}{L_0}. \tag{9}$$

These two quantities θ_f and ε_p, obtained from a detailed analysis at the microscopic scale of the plasticity phenomena developing during the morphological evolution of the film, have been incorporated, in the next part, in the mesoscopic elastic (FvK) theory of thin plates to describe the buckling phenomenon.

5. Modeling of the thin film buckling

A thin film composed of two regions 1 and 2 corresponding to the grains 1 and 2, respectively, is considered in Fig. (5)c. The length of the delaminated part of the grain i is labeled b_i, with $i = 1, 2$ and $b_1 + b_2 \gg h$, in the thin plate hypothesis. For the sake of convenience and unlike the previous numerical analysis, the GB is now located at the origin of the Cartesian axes, the delaminated lengths b_1 and b_2 being thus different in the asymmetric cases. The initial state is taken to be the compressed and planar thin film submitted to the initial stress $\sigma_{xx}^0 = -\sigma_0 = E_f/(1-\nu_f^2)\,\varepsilon_0$, where the elastic strain ε_0 is now defined as the difference between the imposed applied strain ε_a and the plastic strain ε_p, i.e. $\varepsilon_0 = \varepsilon_a - \varepsilon_p < 0$. The Young's modulus E_f and Poisson's ratio ν_f are

the ones provided by the potential chosen for the Al film [22]. They are equal to $E_f = 83.74$ GPa and $\nu_f = 0.321$. In the FvK's theory of thin plates [4, 5, 7], the out-of-plane displacement w_i of the grain i, with respect to the initial state, satisfies the following equilibrium equations:

$$\frac{d^4 w_i}{dx^4} + \alpha^2 \frac{d^2 w_i}{dx^2} = 0, \tag{10}$$

where α is defined as $\alpha = \sqrt{-h\sigma_{xx}/D}$, with $D = E_f h^3/[12(1-\nu_f^2)]$ the bending stiffness and σ_{xx} the stress in the midplane of the delaminated film after buckling, assumed to be constant in both grains to satisfy the mechanical equilibrium conditions at the interface between both grain, i.e. at the GB plane. The σ_{xx} stress and the in-plane displacement u_i of grain i with respect to the initial state can be derived from the compatibility equations:

$$\frac{du_i}{dx} + \frac{1}{2}\left(\frac{dw_i}{dx}\right)^2 = \frac{1-\nu_f^2}{E_f}\sigma_0 - \frac{h^2}{12}\alpha^2. \tag{11}$$

Taking into account the folding effect, the boundary conditions for a clamped film lead to the set of Eqs.:

$$\begin{aligned}
w_1(-b_1) = w_2(b_2) &= 0, && (12)\\
u_1(-b_1) = u_2(b_2) &= 0, && (13)\\
u_1(0) &= u_2(0), && (14)\\
w_1(0) &= w_2(0), && (15)\\
\left.\frac{dw_1}{dx}\right|_{x=-b_1} = \left.\frac{dw_2}{dx}\right|_{x=b_2} &= 0, && (16)\\
\left.\frac{dw_1}{dx}\right|_{x=0} - \left.\frac{dw_2}{dx}\right|_{x=0} &= \beta, && (17)
\end{aligned}$$

with $\beta = \tan(\theta_1) + \tan(\theta_2)$. Solving Eq. (10), the general expression for w_i has been found to be:

$$\begin{aligned}
w_1(x) &= A_1\cos(\alpha x) + B_1\sin(\alpha x) + C_1 x + D_1, && (18)\\
w_2(x) &= A_2\cos(\alpha x) + B_2\sin(\alpha x) + C_2 x + D_2. && (19)
\end{aligned}$$

Since at equilibrium, the buckled film and the grain boundary are free from any applied force [34], the following equilibrium Eq. should be satisfied:

$$\frac{dM_i}{dx} - \alpha^2 D \frac{dw_i}{dx} = 0, \tag{20}$$

with M_i the moment defined as $M_i = -D\frac{d^2 w_i}{dx^2}$. The above Eq. (20) leads to $C_1 = C_2 = 0$. Likewise, the general expression of the horizontal component u_i of the displacement has been found to be from Eq. (11):

$$\begin{aligned}
u_1(x) &= \frac{\alpha}{4}\left[A_1 B_1 - A_2 B_2\right. \\
&+ b_p\alpha\left(A_2^2 + B_2^2\right) - x\alpha\left(A_1^2 + B_1^2\right) \\
&+ A_2 B_2 \cos(2\alpha b_2) - A_1 B_1 \cos(2\alpha x) \\
&+ \frac{1}{2}\left(B_2^2 - A_2^2\right)\sin(2\alpha b_2) - \frac{1}{2}\left(B_1^2 - A_1^2\right)\sin(2\alpha x) \\
&+ \left.\frac{h^2}{3}(b_2 - x) - \frac{1-\nu_f^2}{E_f}\frac{4\sigma_0}{\alpha}(b_2 - x)\right], \qquad (21) \\
u_2(x) &= \frac{\alpha}{4}\left[\alpha(b_2 - x)\left(A_2^2 + B_2^2\right)\right. \\
&+ A_2 B_2\big(\cos(2\alpha b_2) - \cos(2\alpha x)\big) \\
&+ \frac{\left(A_2^2 - B_2^2\right)}{2}\big(\sin(2\alpha x) - \sin(2\alpha b_2)\big) \\
&+ \left.\frac{h^2}{3}(b_2 - x) - \frac{1-\nu_f^2}{E_f}\frac{4\sigma_0}{\alpha}(b_2 - x)\right], \qquad (22)
\end{aligned}$$

where the coefficients A_i, B_i and D_i have been determined with help of Eqs. (12), (13), (14), (15), (16), and (17):

$$A_1 = -\frac{\beta}{2\alpha}\frac{\cos(b_1\alpha)\ \sin\left(\frac{b_2\alpha}{2}\right)}{\sin\left(\frac{(b_1+b_2)\alpha}{2}\right)\ \sin\left(\frac{b_1\alpha}{2}\right)}, \tag{23}$$

$$B_1 = \frac{\beta}{2\alpha}\frac{\sin(b_1\alpha)\ \sin\left(\frac{b_2\alpha}{2}\right)}{\sin\left(\frac{(b_1+b_2)\alpha}{2}\right)\ \sin\left(\frac{b_1\alpha}{2}\right)}, \tag{24}$$

$$D_1 = \frac{\beta}{2\alpha}\frac{\sin\left(\frac{b_2\alpha}{2}\right)}{\sin\left(\frac{(b_1+b_2)\alpha}{2}\right)\ \sin\left(\frac{b_1\alpha}{2}\right)}, \tag{25}$$

$$A_2 = \frac{\beta}{4\alpha}\frac{\cos(b_2\alpha)\ \left(\cos(b_1\alpha) - 1\right)}{\sin\left(\frac{(b_1+b_2)\alpha}{2}\right)\ \sin\left(\frac{b_1\alpha}{2}\right)\ \sin\left(\frac{b_2\alpha}{2}\right)} \tag{26}$$

$$B_2 = -\frac{\beta}{\alpha}\frac{\cos\left(\frac{b_2\alpha}{2}\right)\ \sin\left(\frac{b_1\alpha}{2}\right)^2}{\sin\left(\frac{(b_1+b_2)\alpha}{2}\right)\ \sin\left(\frac{b_1\alpha}{2}\right)}, \tag{27}$$

$$D_2 = \frac{\beta}{\alpha}\frac{1-\cos(b_1\alpha)}{\sin(b_1\alpha)+\sin(b_2\alpha)-\sin((b_1+b_2)\alpha)}. \quad (28)$$

The input parameters required to plot the theoretical profile of the buckle are listed in the Table 2, where the GB positions are related to the d_i quantities defined in the previous paragraph, the values of θ_1, θ_2 and ε_p being obtained from the fully relaxed film (see Fig. (5)b). In Fig. (6), taking $\varepsilon_a = -2.49\%$,

GB position	b_1 (Å)	b_2 (Å)	σ_0 (GPa)	θ_1 (°)	θ_2 (°)	ε_p (%)
d_0	780.99	780.99	1.51	7.45	7.45	-0.292
d_1	867.78	694.20	1.67	4.17	3.34	-0.122
d_2	954.56	607.42	1.61	4.00	6.30	-0.183

Table 2: Input parameters derived form the simulations for different GB positions.

the theoretical profiles of the buckles have been plotted for three particular GB positions, i.e. $d_0 = 0, d_1 = 86.18\mathring{A}$ and $d_2 = 172,94\mathring{A}$ and the corresponding profiles have been found to accurately reproduce the ones obtained from the simulations, justifying thus the introduction of the folding angle and plastic strain quantities in the elastic description of the buckling. Finally, a number of

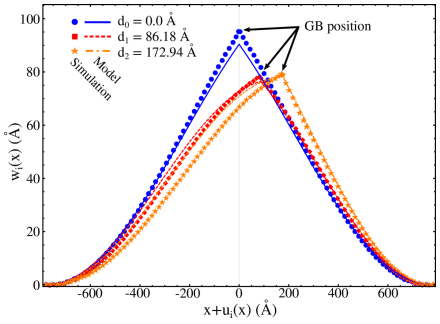

Figure 6: Buckle profiles derived from the model and the simulations for different GB positions, with $\varepsilon_a = -2.49\%$.

simulations has been performed for different values of the GB position d_i, and

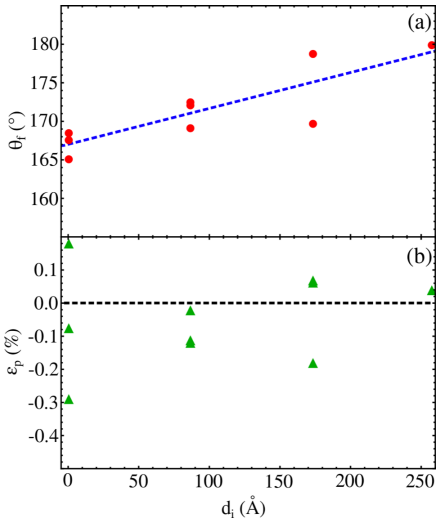

Figure 7: Evolution of, (a) the folding angle θ_f and (b) plastic strain ε_p of the midplane versus d_i.These curves have been obtained from buckling simulations for different GB position d_i.

both θ_f and ε_p parameters obtained from the analysis of the thin film plasticity have been plotted versus d_i in Fig. (7) It is argued that the plasticity of the film during buckling can be captured by these two identified phenomena, i.e. the folding and the irreversible length variation of the delaminated part. It is observed that, as the GB position is modified, the plasticity is distributed differently between the folding and length variation effects, explaining thus the variations of θ_f and ε_p with d_i. Indeed, as d_i increases the GB getting closer to the inflexion region of the buckle profile where the stress gradient through the thickness goes to zero, the stress is decreased near the free surfaces and thus the plasticity is low, θ_f tends to π angle obtained for the classical Euler's column [4, 5]. On this other hand, for the plastic strain ε_p, no real tendency can be underlined since the number of dislocations gliding toward the upper or lower surface may vary depending on the simulation runs. This statement justifies (from the Author's point of view) the dispersion of the ε_p values (positive or negative). Still, as the GB reaches the region of the film sustaining the profile inflexion, ε_p goes to zero, because of the strain decreases and plasticity cancels

(see Fig. (3)b).

6. Conclusion

In this work, the buckling of a delaminated Al thin film under strain has been numerically studied by means of atomistic simulations at finite temperature, when a Σ 51 (551) GB is lying at different positions into the film. It has been clearly evidenced that as the applied strain increases, the plasticity is initiated at the GB and deeply modifies the buckle profiles. Two different plastic mechanisms have been identified. In the upper part of the film under tension, intrinsic stacking faults are generated due to the combination of perfect dislocations with partial Shockley's dislocations coming from the top surface. In the lower part of the film under compression, extrinsic stacking faults are formed due to the dissociation of the perfect dislocations in partial Shockley's dislocations which glide in two successive planes. Due to this GB plasticity, the film is folded (θ_f) and plastically strained (ε_p). In the framework of the FvK theory of thin plates, taking into account the plasticity parameters θ_f and ε_p in the mesoscopic description of the buckling, the final shape of the film has been accurately described. It is also emphasized that the plasticity is also dependent on the initial GB position since the stress distribution varies along the horizontal axis of the film. The next step of this work would be to carry out MD simulations for GB structures introduced in other materials than Al, in order to determine whether or not the thin film folding is governed by equivalent plasticity mechanisms as the ones identified in the Al case. For example, additional simulations have already been performed in gold crystals (not shown) with the same dimensions and equivalent GB configuration. It has been confirmed that plastic mechanisms are governed by the glide of perfect dissociated dislocations (leading and trailing partials), rather than only partial dislocations and extrinsic faults, in the compressed area. Unlike aluminum, the perfect crystal has been found to be fully recovered in gold. Likewise, it still has to be investigated if there exists a more quantitative relation between the folding angles, the plastic

strains and the buckle morphologies from one part and the material plasticity on the other.

The authors acknowledge the supercomputer facilities of the Mesocentre de calcul Poitou-Charentes.

References

[1] F. Motazedian, Z. Wu, J. Zhang, B. S. Shariat, D. Jiang, M. Martyniuk, Y. Liu, H. Yang, Determining intrinsic stress and strain state of fibre-textured thin films by X-ray diffraction measurements using combined asymmetrical and bragg-brentano configurations, Materials and Design 181 (2019) 108063. doi:https://doi.org/10.1016/j.matdes.2019.108063. URL http://www.sciencedirect.com/science/article/pii/S0264127519305015

[2] E. Chason, B. W. Sheldon, L. B. Freund, J. A. Floro, S. J. Hearne, Origin of compressive residual stress in polycrystalline thin films, Phys. Rev. Lett. 88 (2002) 156103. doi:10.1103/PhysRevLett.88.156103.
URL https://link.aps.org/doi/10.1103/PhysRevLett.88.156103

[3] P. Godard, D. Faurie, T. Sadat, M. Drouet, D. Thiaudière, P. Renault, X-ray diffraction and stress relaxations to study thermal and stress-assisted annealings in nanocrystalline gold thin films, Acta Materialia 173 (2019) 87 – 95. doi:https://doi.org/10.1016/j.actamat.2019.04.024. URL http://www.sciencedirect.com/science/article/pii/S1359645419302265

[4] J. Hutchinson, M. Thouless, E. Liniger, Growth and configurational stability of circular, buckling-driven film delaminations, Acta Metallurgica et Materialia 40 (2) (1992) 295 – 308. doi:https://doi.org/10.1016/0956-7151(92)90304-W.

[5] J. Hutchinson, Z. Suo, Mixed mode cracking in layered materials, Vol. 33

of Advances in Applied Mechanics, Elsevier, 1991, pp. 119 – 193. doi:https://doi.org/10.1016/S0065-2156(08)70164-9.

[6] G. Gioia, M. Ortiz, Delamination of compressed thin films, Vol. 29 of Advances in Applied Mechanics, 1997, pp. 63 – 191.

[7] L. B. Freund, S. Suresh, Thin Film Materials: Stress, Defect Formation and Surface Evolution, Cambridge University Press, 2004. doi:10.1017/CBO9780511754715.

[8] B. Audoly, Stability of straight delamination blisters, Phys. Rev. Lett. 83 (1999) 4124–4127. doi:10.1103/PhysRevLett.83.4124.

[9] G. Parry, A. Cimetière, C. Coupeau, J. Colin, J. Grilhé, Stability diagram of unilateral buckling patterns of strip-delaminated films, Phys. Rev. E 74 (2006) 066601. doi:10.1103/PhysRevE.74.066601.

[10] J. Y. Faou, G. Parry, S. Grachev, E. Barthel, How does adhesion induce the formation of telephone cord buckles?, Phys. Rev. Lett. 108 (2012) 116102. doi:10.1103/PhysRevLett.108.116102.

[11] G. Parry, S. Hamade, J. Durinck, C. Coupeau, J. Colin, Influence of interface steps on the buckle delamination of thin films, J. Mech. Phys. 132 (2019) 103698. doi:https://doi.org/10.1016/j.jmps.2019.103698.

[12] M. Cordill, F. Fischer, F. Rammerstorfer, G. Dehm, Adhesion energies of cr thin films on polyimide determined from buckling: Experiment and model, Acta Materialia 58 (16) (2010) 5520 – 5531. doi:https://doi.org/10.1016/j.actamat.2010.06.032.
URL http://www.sciencedirect.com/science/article/pii/S1359645410003976

[13] K. Wu, Y. Xia, H. Yuan, J. Zhang, G. Liu, J. Sun, Cohesive and adhesive properties of nanocrystalline ti thin films on polyimide substrates, Materials Science and Engineering: A 744 (2019) 746 – 753.

doi:https://doi.org/10.1016/j.msea.2018.12.089.
URL http://www.sciencedirect.com/science/article/pii/S0921509318317684

[14] K. Wu, Y. Wang, H. Yuan, J. Zhang, G. Liu, J. Sun, Unique buckling and post-buckling behavior of Cu–Zr amorphous films on compliant substrates, Materials Letters 237 (2019) 118 – 121. doi:https://doi.org/10.1016/j.matlet.2018.11.095.
URL http://www.sciencedirect.com/science/article/pii/S0167577X18318603

[15] K. Wu, J. Zhang, G. Liu, P. Zhang, P. Cheng, J. Li, G. Zhang, J. Sun, Buckling behaviors and adhesion energy of nanostructured Cu/X (X=Nb, Zr) multilayer films on a compliant substrate, Acta Materialia 61 (20) (2013) 7889 – 7903. doi:https://doi.org/10.1016/j.actamat.2013.09.028.
URL http://www.sciencedirect.com/science/article/pii/S1359645413007131

[16] K. Wu, J. Zhang, J. Li, Y. Wang, G. Liu, J. Sun, Length-scale-dependent cracking and buckling behaviors of nanostructured Cu/Cr multilayer films on compliant substrates, Acta Materialia 100 (2015) 344 – 358. doi:https://doi.org/10.1016/j.actamat.2015.08.055.
URL http://www.sciencedirect.com/science/article/pii/S1359645415006321

[17] J. Colin, C. Coupeau, J. Durinck, J. Grilhé, Buckling and cracking of Y_2O_3 thin films at grain boundaries, Phys. Rev. B 78 (2008) 153411. doi:10.1103/PhysRevB.78.153411.
URL https://link.aps.org/doi/10.1103/PhysRevB.78.153411

[18] J. Colin, C. Coupeau, J. Grilhé, Plastic folding of buckling structures, Phys. Rev. Lett. 99 (2007) 046101. doi:10.1103/PhysRevLett.99.046101.
URL https://link.aps.org/doi/10.1103/PhysRevLett.99.046101

[19] J. Li, Disclination model of high angle grain boundaries, Surface Science 31 (1972) 12 – 26. doi:https://doi.org/10.1016/0039-6028(72)90251-8.
URL http://www.sciencedirect.com/science/article/pii/0039602872902518

[20] J. Durinck, C. Coupeau, J. Colin, J. Grilhé, Molecular dynamics simulations of buckling-induced plasticity, Applied Physics Letters 93 (22) (2008) 221904. arXiv:https://doi.org/10.1063/1.3033552, doi:10.1063/1.3033552.
URL https://doi.org/10.1063/1.3033552

[21] S. Plimpton, Fast parallel algorithms for short-range molecular dynamics, Journal of Computational Physics 117 (1) (1995) 1 – 19. doi:https://doi.org/10.1006/jcph.1995.1039.
URL http://www.sciencedirect.com/science/article/pii/S002199918571039X

[22] R. R. Zope, Y. Mishin, Interatomic potentials for atomistic simulations of the Ti-Al system, Phys. Rev. B 68 (2003) 024102. doi:10.1103/PhysRevB.68.024102.
URL https://link.aps.org/doi/10.1103/PhysRevB.68.024102

[23] J. M. Penisson, A. Bourret, High–resolution study of [011] low–angle tilt boundaries in aluminium, Philosophical Magazine A 40 (6) (1979) 811–824. arXiv:https://doi.org/10.1080/01418617908234876, doi:10.1080/01418617908234876.
URL https://doi.org/10.1080/01418617908234876

[24] A. P. Sutton, V. Vitek, J. W. Christian, On the structure of tilt grain boundaries in cubic metals i. symmetrical tilt boundaries, Philosophical Transactions of the Royal Society of London. Series A, Mathematical and Physical Sciences 309 (1506) (1983) 1–36. arXiv:https://royalsocietypublishing.org/doi/pdf/10.1098/rsta.1983.0020, doi:10.1098/rsta.1983.0020.

URL https://royalsocietypublishing.org/doi/abs/10.1098/rsta.1983.0020

[25] Y. Cheng, D. Weygand, P. Gumbsch, Simulation of small-angle tilt grain boundaries and their response to stress, Computational Materials Science 45 (3) (2009) 783 – 787, proceedings of the 17th International Workshop on Computational Mechanics of Materials. doi:https://doi.org/10.1016/j.commatsci.2008.05.028.
URL http://www.sciencedirect.com/science/article/pii/S0927025608002632

[26] L. Zhang, C. Lu, Y. Shibuta, Shear response of grain boundaries with metastable structures by molecular dynamics simulations, Modelling and Simulation in Materials Science and Engineering 26 (3) (2018) 035008. doi:10.1088/1361-651x/aaacaa.
URL https://doi.org/10.1088%2F1361-651x%2Faaacaa

[27] W. T. Read, W. Shockley, Dislocation models of crystal grain boundaries, Phys. Rev. 78 (1950) 275–289. doi:10.1103/PhysRev.78.275.
URL https://link.aps.org/doi/10.1103/PhysRev.78.275

[28] J. Hutchinson, Z. Suo, Mixed mode cracking in layered materials, Vol. 29 of Advances in Applied Mechanics, Elsevier, 1991, pp. 63 – 191. doi:https://doi.org/10.1016/S0065-2156(08)70164-9.
URL http://www.sciencedirect.com/science/article/pii/S0065215608701649

[29] V. Yamakov, D. Wolf, S. R. Phillpot, A. K. Mukherjee, H. Gleiter, Dislocation processes in the deformation of nanocrystalline aluminium by molecular-dynamics simulation, Nature Materials 1 (1) (2002) 45–49. doi:10.1038/nmat700.
URL https://doi.org/10.1038/nmat700

[30] J. Wang, H. Huang, Shockley partial dislocations to twin: Another formation mechanism and generic driving force, Applied Physics Letters

85 (24) (2004) 5983–5985. arXiv:https://doi.org/10.1063/1.1835549, doi:10.1063/1.1835549.
URL https://doi.org/10.1063/1.1835549

[31] J. Hirth, J. Lothe, Theory of Dislocations, Krieger Publishing Company, 1982.
URL https://books.google.fr/books?id=LFZGAAAAYAAJ

[32] J. Grilhé, K. Seshan, J. Washburn, On the possibility of nucleating loops with burgers vector (DC') by the clustering of interstitials, Radiation Effects 27 (1-2) (1975) 115–118. arXiv:https://doi.org/10.1080/00337577508233018, doi:10.1080/00337577508233018.
URL https://doi.org/10.1080/00337577508233018

[33] M. Fnaiech, F. Louchet, B. Jouffrey, On the structure of multiple frank loops in quenched aluminium-silicon alloys, Acta Metallurgica 29 (2) (1981) 383 – 391. doi:https://doi.org/10.1016/0001-6160(81)90164-4.
URL http://www.sciencedirect.com/science/article/pii/0001616081901644

[34] M.-H. Zhao, F. Yang, T.-Y. Zhang, Delamination buckling in the microwedge indentation of a thin film on an elastically deformable substrate, Mechanics of Materials 39 (9) (2007) 881–892. doi:10.1016/j.mechmat.2007.03.003.